Desalination and Water Treatment
www.deswater.com

doi: 10.5004/dwt.2019.23491

140 (2019) 302–311
February

Carbon biogenic with iron nanoparticles for removal of As(V) from water

G. García-Rosales[a,*], L.C. Longoria-Gándara[b], P. Ávila-Pérez[c], M.C. López-Reyes[c]

[a]*Instituto Tecnológico de Toluca, Departamento de posgrado. Ex-rancho la virgen S/N, C.P. 50120, Metepec, México, email: gegaromx@yahoo.com.mx*
[b]*Division for Latin America/Department of Technical Cooperation International Atomic Energy Agency. Wagramer Strasse 5, P.O. Box 100, A-1400 Vienna, Austria*
[c]*Instituto Nacional de Investigaciones Nucleares. Dirección de Investigación Tecnológiva. Carretera México-Toluca S/N, La Marquesa, Ocoyoacac, México C.P. 52750*

Received 11 May 2018; Accepted 18 November 2018

ABSTRACT

This manuscript presents evaluation of arsenic adsorption by carbon (Cb) and a carbonaceous material with iron nanoparticles (CbFe), coming from the pineapple peel (*Ananas comosus* (L.) Merr.) crown. Scanning electron microscopy results showed formation of three structures types in CbFe: spheres, filaments and spherical nanoparticles with an average diameter of 38 nm. CbFe material has a 167 m^2/g specific area, 7±1 sites/nm^2 site density and pH_i = 11 isoelectric point, while Cb material presents values of 98.80 m^2/g, 5 ± 1 sites/nm^2 and pH_i = 10 ± 0.6, respectively. Arsenic adsorption was evaluated for both materials; the kinetic equilibrium was obtained at 8 h, removing 138.5 mg As/kg by CbFe and 96.95 mg As/kg by Cb. Experimental data were best adjusted to a pseudo-second order model, indicating that removal of As(V) due to a chemisorption process. The sorption isotherms were adjusted to model Freundlich with R^2 = 0.8797 and R^2 = 0.9671, respectively. Results showed that both materials are a viable option for arsenic (V) adsorption in aqueous phase.

Keywords: Arsenic; Nanoparticles; Iron; Carbon; Adsorption

1. Introduction

Arsenic (As) is present as organic and inorganic compounds in nature, with oxidation states III and V and its mobility in the environment is mainly controlled by chemical, biological and physico-chemical phenomena [1,2]. Arsenic at concentrations ranging from a few micrograms to milligrams per litre in drinking water may cause acute toxicity effects in people through strong arsenic binding to proteins; arsenic in small amounts may have adverse effects on sensitive human groups such as pregnant women or infants [3]. According to the World Health Organization (WHO), the arsenic limit in water is 10 μg/L. However, in some countries the current regulation allows up to 25 μg L^{-1} [4]. Arsenic as a pollutant in the environment has motivated the development and application of different removal technologies, such as coagulation–flocculation [5], electrolysis [6], electrocoagulation [7], membrane technologies [8], biological methods [9] and adsorption processes [10]. Adsorption is one of the most popular methods as it is currently considered highly efficient because of simplicity, treatment stability and cost effectiveness. Oxides, activated carbon, red mud, alumina [11,12] and biomass [13] are materials extensively used in the sorption process for the removal of As(V) from water. However, in previous decades nanotechnology has become increasingly important because it offers indisputable advantages to almost every area of expertise, including environmental nano-remediation [14]. Especially the zero-valence iron and iron oxide nanoparticles with different polymorph structures that have unique physical and chemical properties which are useful for a wide variety of applications and are effective in arsenic removing from aqueous phase

* Corresponding author.

[15–17]. There are two different methods that can be used to produce nanomaterials: top-down and bottom-up methods. The first method consists in the reduction of iron particle size through mechanical and/or chemical processes, and the second includes specific equipment and it is associated with high energy costs. In the bottom-up method, two distinct paths can be followed: traditional and green production methods. Traditional method involves the reaction between iron(III) or iron(II) solutions with sodium borohydride [18]. In general, wet syntheses result in complex aqueous chemical reactions, such as hydrolysis, oxidation and polymorphic transformations. Consequently, new processes have been devised in the green synthesis of iron nanoparticles using natural products. The use of biomass provides several advantages when compared with the traditional method: (i) the polyphenolic matrix can act as a capping agent that protects the iron nanoparticles from premature oxidation [19] and (ii) the natural products valorization, such as pineapple peel, that in some cases, are considered wastes. Recently zero valent iron nanoparticles were synthesized from the leaf extracts of *Eucalyptus globules* and were applied in the efficient adsorption of Cr(VI) [20]. Application of Fe and Fe/Pd bimetallic nanoparticles from green tea extract for the reductive degradation of chlorinated organic has been reported [21]; Es´haghi [22] reports the synthesis and functionalization of magnetic iron nanoparticles using green chemistry (olive oil) for the extraction of nickel from environmental samples. Nanoparticles in the aqueous media tend to aggregate due to magnetic properties which limit the radius of influence and hinder the recovery during aqueous phase. An alternative is to use a material that serves as a nanoparticles support and facilitates the contact with the pollutant to be removed. The immobilization of the synthesized nanoparticles onto porous solids is used to avoid the operational problem previously mentioned. In addition, immobilization helps to enhance certain properties of the materials such as stability and mechanical strength. Different materials have been used as supports for different nanoparticle systems with regard the treatment of effluents [23–25]. However it has been observed that the combination of magnetic nanoparticles with carbon has many unique properties including good thermal stability, a wide electrochemical (conductivity) window, turnable miscibility and good extraction capability, which makes them promising materials for heavy metal removal, and pollutants adsorption [26]. Previous studies realized by Park et al. [27] show that powered activated carbons impregnated with iron nanoparticles removed bisphenol effectively in the presence of natural organic matter; Yu et al. [28] used magnetic iron oxide nanoparticles functionalized multi-walled carbon nanotubes for toluene, ethylbenzene and xylene removal from aqueous solution. Yadav et al. [29] presented a study of phenol removal from water by catalytic wet air oxidation using carbon bead–supported iron nanoparticle containing carbon nanofibres. Recently, another study is reported by Wang et al. [30] where porous three-dimensional graphene (3DG) is prepared by chemical vapour deposition and is used as a matrix to support nanoscale zero-valent iron (nZVI) particles for azo dye degradation; Jabeen et al. [31] and Guo et al. [32] utilized 2D graphene sheets as a supporting template to prepare nZVI-decorated graphene composites. These hybrid materials demonstrated a higher capability for Cr(VI) and methyl blue removal.

The aim of this study is to obtain a carbon biomaterial conditioned with iron nanoparticles starting from the pineapple peel and to evaluate their arsenic adsorption capacity in an aqueous phase.

2. Experimental setup

2.1. Synthesis

The schematic preparation of the Cb and CbFe is shown in Fig. 1. For this study, pineapples (*Ananas comosus* (L.) Merr.) obtained from Mexico were used. In the laboratory, the pineapple peel was washed several times with double-distilled water to remove surface impurities and dried at 25°C for 24 h. After, it was ground and sieved in order to obtain a size of 0.85 mm (mesh 20). The pineapple peel was then repeatedly washed with deionized water at 120°C for 15 min to completely remove the brown discolouration and then it was dried at 25°C.

To obtain CbFe, the chemicals used were of analytical grade. A mixture of 12 mL $C_{28}H_{30}Na_8O_{27}$ (carboxymethyl cellulose sodium; 2% w/w; Sigma-Aldrich®) (St. Louis Missouri, USA), and 18 mL of Fe $(NO_3)_3$ $9H_2O$ (iron(III) nitrate nonahydrate; 0.06 M; Sigma-Aldrich®, 98%) with 6 mL of $(CH_2)_6N_4$ (hexamethylenetetramine; 0.5 M; Sigma-Aldrich®, 99.9%) were combined in a reactor with argon (Ar) atmosphere and with constant agitation. Once the mixture was homogenized, 3 g (previously established amount) of pineapple peel (mesh 20) was added to the mixture and agitated in an ultrasonic bath for 45 min, prior to being placed in a fused alumina crucible, which was then subsequently introduced into a quartz tube under Ar within a furnace (Lindberg®/Blue Model CC58114A-1) for 180 min at pyrolysis time at 650°C.

2.2. Morphology, surface characterization and crystallographic structure

In order to obtain the morphology and chemical structure of carbon biomaterials, a scanning electron microscope model JEOL® (Japan) JSM-6610 LV at 25 kV was used. The samples were mounted on an aluminum holder with aluminum conductive tape and it was then covered with a layer of gold approximately 150 Å thick using a sputter coater Desk II model, Denton Vacuum (China). The elemental chemical compositions of the samples were then determined by energy dispersive X-ray spectroscopy using an OXFORD® spectrometer (UK). The main chemical groups were studied by Fourier transform infrared spectroscopy (FTIR) using a Nicolette® 550 infrared spectrophotometer (USA) with KBr discs. The samples were scanned from 4,000 to 400 cm^{-1}. The crystal phases of Cb and CbFe were analyzed by XRD patterns using a Siemens-D-5000S® diffractometer (Germany) with a copper anode X-ray tube (λ = 1.543 Å).

The specific surface area was determined by N_2 Brunauer–Emmett–Teller (BET) nitrogen adsorption method with a BELPREP-flow II BEL JAPAN® Inc. surface analyzer. Dried and degassed samples were analyzed by N_2 adsorption–desorption multipoint method at room temperature. The point of zero charge (pH_{pzc}) was determined by mass titration experiments. Respectively, different amounts of Cb and CbFe (0–2 g) were mixed with 10 mL of water in polypropylene tubes. The resulting suspension was stirred for 24 h to

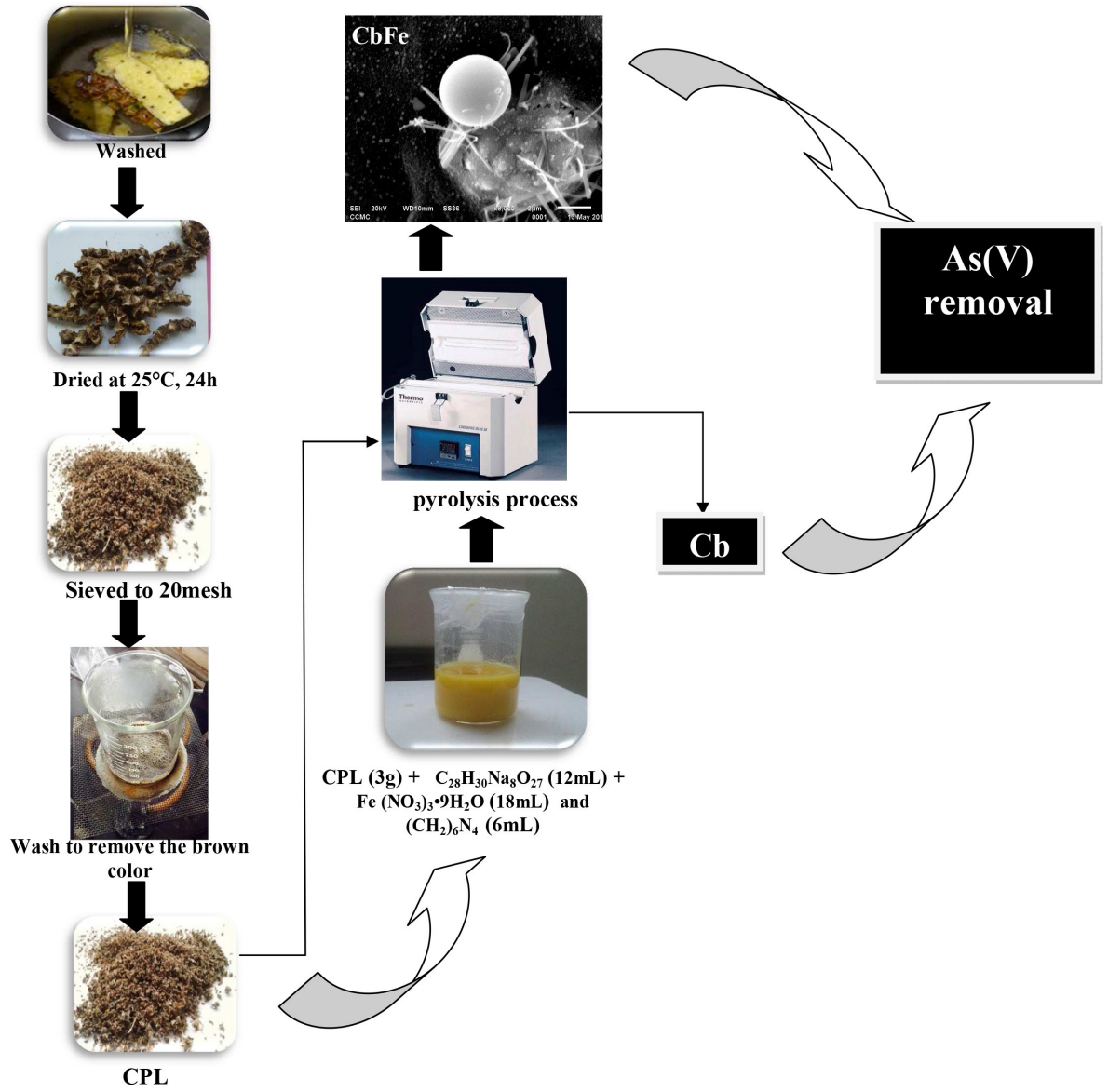

Fig. 1. Schematic experimental representation of the process used to prepare the CbFe and its utilization for the removal of heavy metals.

allow the hydration of the solid surface before centrifugation at 3,500 rpm for 10 min. Then the pH was then measured in a Denver Instruments® potentiometer (USA).

To determine active sites, potentiometric titrations of Cb and CbFe (300 mg), respectively, were performed in an $NaClO_4$ (0.1 Mol/L) solution at 25°C in an argon atmosphere. The suspension was acidified with $HClO_4$ (0.1 Mol/L) at an initial pH = 2 and it was then stirred for 24 h, with the titration being added NaOH (0.1 Mol/L).

2.3. Arsenic adsorption

2.3.1. Effect of initial pH, concentration and contact time

An arsenic solution stock was prepared by dilution of 10 mL As_2O_5, Titrisol, MERCK® 1,000 mg/L to 100 mg/L with deionized water. This solution was further diluted to the concentration required for each experiment. In order to evaluate the effect of pH on the As(V) adsorption process the experiments were carried out in a batch mode, where 30 mg of Cb or CbFe were mixed with 10 mL of 30 mg/L (As_2O_5) solution in polypropylene tubes at pH values from 1 to 7, the suspensions were shaken in a water bath for 24 h at 20°C, NaOH and HNO_3 0.1 M solutions were used to adjust the pH of the mixtures in all the experiments. TTo evaluate the effect of ion concentration on the removal of As (V), the samples were prepared at concentrations between 3 and 40 mg L^{-1} in 10 mL solution using 30 mg of Cb or CbFe, respectively. Whilst for sorption kinetics, each material was put in contact with 10 mL of a 30 mg L^{-1} arsenic solution at $pH_i = 6 \pm 0.1$ at 20°C, the experiments were performed at different contact times. The arsenic concentration in the solids carbonaceous materials after the adsorption process was determined by NAA (neutron activation analysis) as described below.

2.3.2. Arsenic concentration: neutron activation analysis

0.02 g of Cb or CbFe coming from the arsenic adsorption process was encapsulated in polyethylene containers for irradiation. An arsenic standard solution of 30 μL of As_2O_5 Tridisol, Merck® (1,000 mg L^{-1}) was deposited on a piece of paper Whatman 41 low in ash and also it was encapsulated in a polyethylene container for irradiation. The encapsulated samples were irradiated for 2 h with thermal neutrons in the Fixed Irradiation System (SIRCA) with a neutron flux of 9×10^{12} n/cm²·s in the TRIGA Mark III (USA) nuclear reactor of the National Institute for Nuclear Research in Mexico. The irradiated samples were measured in a gamma spectrometer equipped with a hyper-pure Ge detector ORTEC® (The Netherlands).

3. Results

3.1. Morphology, crystallinity, surface properties and functional groups

Fig. 2(a) shows the Cb mycography, where the formation of iron nanoparticles on the surface of the carbon cannot be observed. The opposite happens for CbFe where small

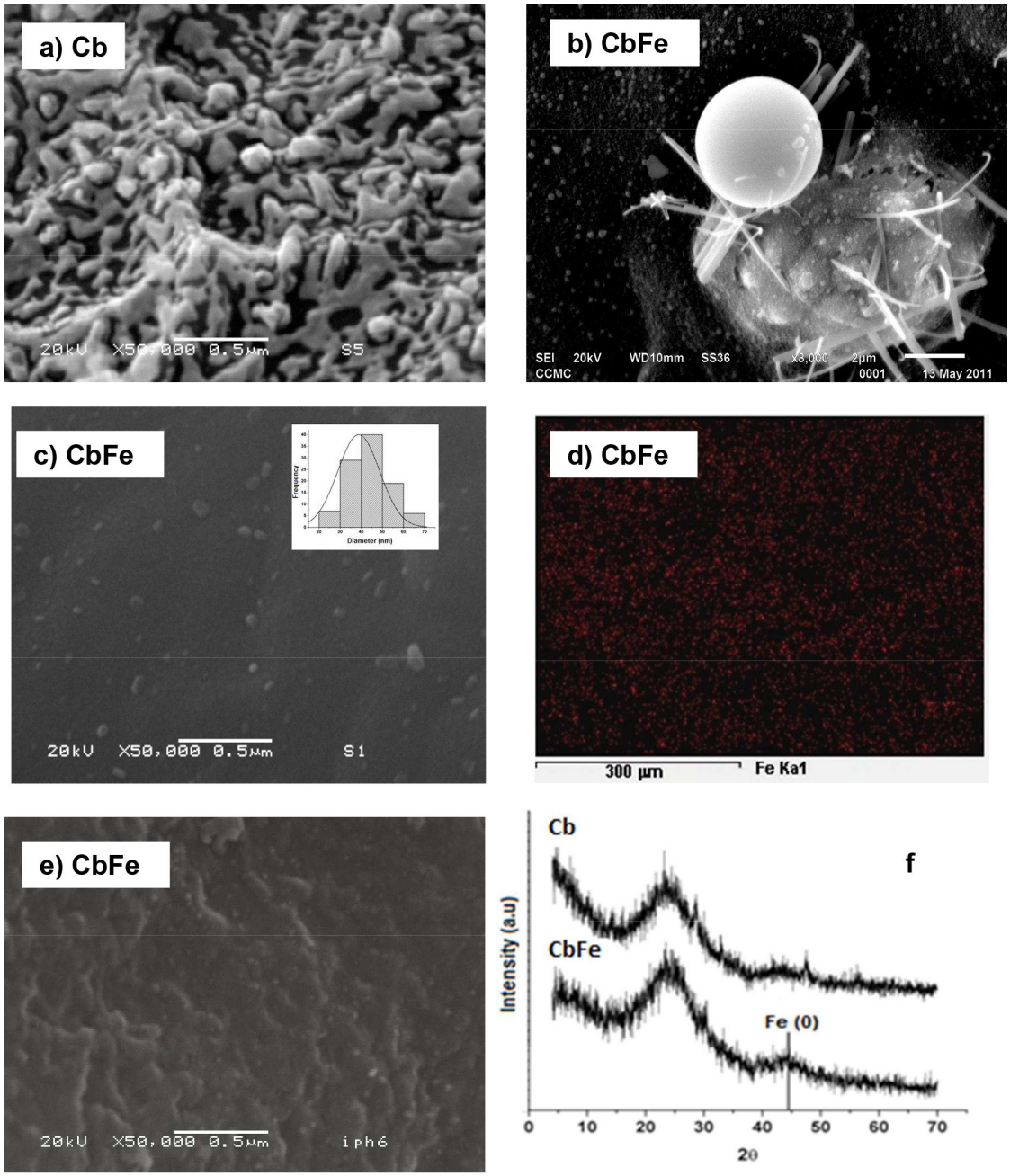

Fig. 2. (a) Carbon surface of Cb; (b) carbonaceous material with iron nanoparticles (CbFe); (c) amplification of CbFe; (d) iron mapping in CbFe; (e) CbFe material after the sorption process; (f) Ray diffraction spectrum of CbFe and Cb materials.

spherical particles of nanometric size appear on the surface carbonaceous material, this can be attributed to the formation of iron nanoparticles. When pineapple peel is subjected to the process of pyrolysis, different structures are formed and can be observed that the formation of spheres with 6 μm diameter and filaments emerging from the silicon nodules of 108 nm length with a 14.6 nm width. The filaments and spheres structures are formed on the top of silicon nodules that form the shell structure of pineapple (Fig. 2(b)). The pineapple peel presents small structures on their surface with around 150 and 200 individual fruits attached to a central axis [33]. In Fig. 2(c) it is observed with more detail the presence of a sphere formed during the pyrolysis process, small spherical iron particles appear evenly dispersed across the carbon surface with an average diameter of 38.8 nm and homogeneously distributed in the carbon structure. This effect results from the chemical preparation of pineapple peel, first through the reagent penetration in the entire structure of the biomaterial and second, during the pyrolysis process where carbon and nanoparticles were formed at the same time. The elemental composition analysis of CbFe shows the presence of C (75.92%), O (16.03%), Na (1.60%), Mg (0.23%), Al (0.20%), Si (1.04%), P (0.56%), S (0.54%), K (0.43%), Ca (1.44%) and Fe (2.01%). The presence of Na, Mg, Al, Si, P, S, K is due to the process of obtaining nutrients, the plant takes those elements from the soil. The distribution of iron in the carbonaceous material is homogenous according to the mapping performed (Fig. 2(d)). After the adsorption process (Fig. 2(e)), iron nanoparticles remain in the structure of the carbonaceous material and the surface of material does not present changes due to the pH solution value, neither the stirring process, showing that it is stable and viable to be used in the removal of As in aqueous phase [27].

The XRD) results showed that Cb and CbFe materials have an amorphous structure. Fig. 2(f) shows that the CbFe material presents two peaks, one at 25° and the other at 45° in 2θ scale with centroide in 24° attributed to the Fe^0 (ICDDPDF2007 03-065-4899) and the Cb material only presented one peak at 25° in 2θ scale. The CbFe material showed 7 ± 0.1 sites/nm^2 whilst the Cb material 5 ± 0.1 sites/nm^2. When the two materials are compared, a difference of 2 ± 0.1 sites/nm^2 is observed and it can be to do with the presence of iron nanoparticles in the carbonaceous material. The isoelectric point is similar in both materials; in Cb at pH = 10.6 and CbFe at pH = 11, showing that the iron nanoparticles did not alter the isoelectric point of the material, probably because the low amount of iron. In both materials, the surface charge is positive, which is favourable for the sorption of As(V), such as: $HAsO_4^{2-}$ and AsO_4^{3-} [2].

In Table 1 it can be observed that the specific area of CbFe is significantly greater than Cb, whilst the pore diameter does not change in both materials; however the pore volume in CbFe is greater than Cb. This can be attributed to the carbon conditioned with the iron nanoparticles obtained at the same time during the pyrolysis process. The difference of 68.2 m^2/g in the specific area between Cb and CbFe shows that the presence of iron nanoparticles favours this parameter for CbFe, another factor that contributes to this increase is the pore volume for Cb is less than CbFe. According to the results, Cb and CbFe can be considered as mesoporous materials, because the pore diameter is in the range of 2–50 nm [34].

Table 1
Specific area, volume and pore size of carbonaceous materials

Material	Specific area (m^2/g)	Pore volume (nm)	Pore diameter (nm)
Cb	98.80	0.0598	2.42
CbFe	167.00	0.1053	2.52

The FTIR spectrum of the CbFe indicates the presence of various functional groups. In Figs. 3(a) and (e) the pineapple peel (CP) shows the following bands: 3,348 cm^{-1} (OH); 2,932–2,855 cm^{-1} (C–H); 1,735 cm^{-1} (C=O); 1,622 cm^{-1} (C=C); 1,370 cm^{-1} (O–H and C=O); 1,238 cm^{-1} (ester linkages that are coming from cellulose, hemicellulose and lignin). The band at 1,034 cm^{-1} confirms the presence of C–O that corresponds to phenol groups and is common in the lignocellulosic materials. During the washing of the pineapple peel, a decrease in intensity of the first band at 3,348 cm^{-1} which is attributed to the loss of phenolic compounds (Figs. 3(b) and (f)) [35–38], whilst the material is conditioned with iron solution and carboxymethyl cellulose sodium, the intensity of the bands located at 3,348 and 1,034 cm^{-1} increased (Figs. 3(c) and (g)) complexes are formed. No significant change is observed in the bands located at 2,932 and 2,855 cm^{-1} between the CP and Cb materials. However in CbFe material, it is noted that the presence of a doublet due to the Fe interaction near 500 cm^{-1} [39]. In Fig. 3(h) two bands are observed at 3,771 and 3,552 cm^{-1} that are corresponding to the NH and NH_2 groups, and the double band at 2,984 and 2,895 cm^{-1} is assigned to the tension C–H of methyl and methylene groups of lignin; the isonitrile groups are located at 2,362 and 2,334 cm^{-1}. Additionally the bands located at 2,100; 1,735 and 1,538 cm^{-1}, are assigned to isocyanate groups (N=C=O, C=O and C=C). It is observed that some bands decrease, suggesting the rupture of links during the pyrolysis of cellulose, hemicellulose and lignin.

3.2. Adsorption studies

3.2.1. pH effect

Fig. 4(a) presents the isotherm in function of pH change of the solution at an As(V) initial concentration of 30 mg L^{-1} and it is observed that Cb material removes less As(V) than CbFe material. The maximum removal is observed at pH = 2 where the chemical species H_3AsO_4 and $H_2AsO_4^-$ are predominate and the chemical specie $H_2AsO_4^-$ has a greater tendency to be absorbed in the surface material so the percentage of removal increases. The results can be related to the isoelectric point of both materials as they have a net positive electrical charge on the surface and it favours the arsenic removal at acid pH in relation with the species of As(V) present in the solution. At pH = 3, the chemical species H_2AsO_4 predominates, however the removal of As(V) decreases [40–42]. In Fig. 4(b) it is observed that CbFe removes more As(V) than Cb at all the contact times and both materials have a removal peak at 8 h. However, the remotion capacity is higher for the material containing iron nanoparticles with 65% removal of arsenic in the first minutes of contact. This behaviour shows that the CbFe material is more efficient than the Cb material.

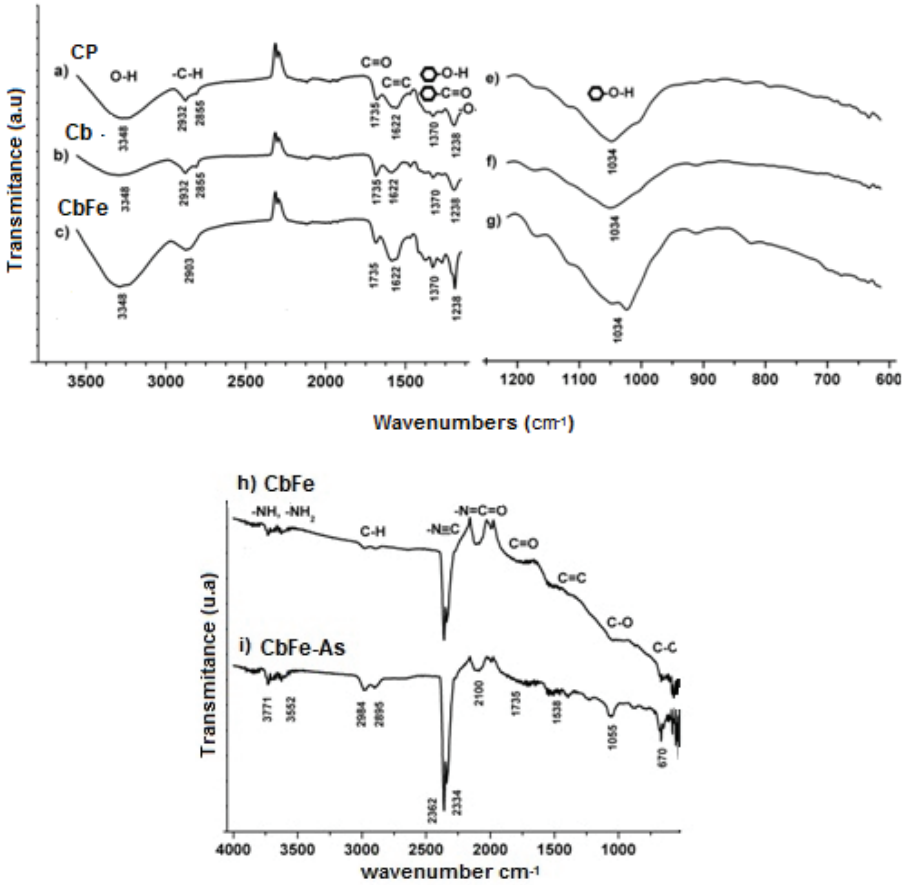

Fig. 3. Infrared spectra from 4,000 to 1,200 cm^{-1} and from 1,200 to 600 cm^{-1}; (a,e) CP; (b,f) Cb; (c,g) CbFe; (h) CbFe infrared spectrum before As(V) sorption process; (i) after As(V) sorption process.

The experimental data for As(V) adsorption for both materials were fitted by means of three kinetic models: diffusion-chemistry adsorption, pseudo-first-order and pseudo-second-order models. The best fit to the As(V) adsorption data in both materials were obtained with a pseudo-second-order model [43,44]. The kinetic rate equation is represented mathematically by Eq. (1) as follows:

$$t/q_t = 1/k_2 q_e^2 + (1/q_e)*t \quad (1)$$

where k_2 (g/mg min) is the pseudo-second-order rate constant of adsorption, q_e is the adsorption capacity at equilibrium (mg/g) and q_t is the amount of arsenic ions removed at time t (mg/g). The values of each parameter are presented in Table 2.

The results show that the material adsorption capacity is proportional to the number of active sites on the surface, which favours a chemisorption process. The q_e and k_2 are 1.5 and 2 times higher for CbFe than to Cb in the adsorption of As(V) and shows that CbFe has a better adsorption capacity for As(V) [45,46].

Fig. 4(c) shows the adsorption isotherms of CbFe and Cb materials, where a maximum arsenic sorption of 67% and 75%, respectively, can be observed. The adsorption experimental data were adjusted to Freundlich and Langmuir models in order to explain the As(V) adsorption behaviour by the carbonaceous materials. In Table 3, it is observed that the Freundlich model best describes the adsorption process ($R^2 > 0.87$) suggesting the formation of successive layers of adsorbate on the material surface in a heterogeneous medium [47].

The Freundlich model is formulated in Eq. (2):

$$q_e = K_F C_e^{1/n} \quad (2)$$

where q_e is the mass ratio of the adsorbed solute on the adsorbent (mg g^{-1}); C_e is the equilibrium solute concentration (mg L^{-1}); K_F is the Freundlich constant representing the adsorption capacity and strength of the adsorptive bond and n is the heterogeneity factor representing the bond distribution. The value of $1/n$ is less than one for the arsenic adsorption on the nanocomposite at the studied temperature, showing that the process of adsorption is favourable.

Table 4 compares the arsenic adsorption capacity of Cb and CbFe materials with other adsorbents, and it can be observed that the capacity of the carbonaceous materials is high. The parameter values show that Cb and CbFe materials could be used as a useful biosorbent for the As(V) removal from wastewaters. An advantage of the use of the material obtained in this study is its low cost compared with other carbons because it is obtained starting an organic waste, which

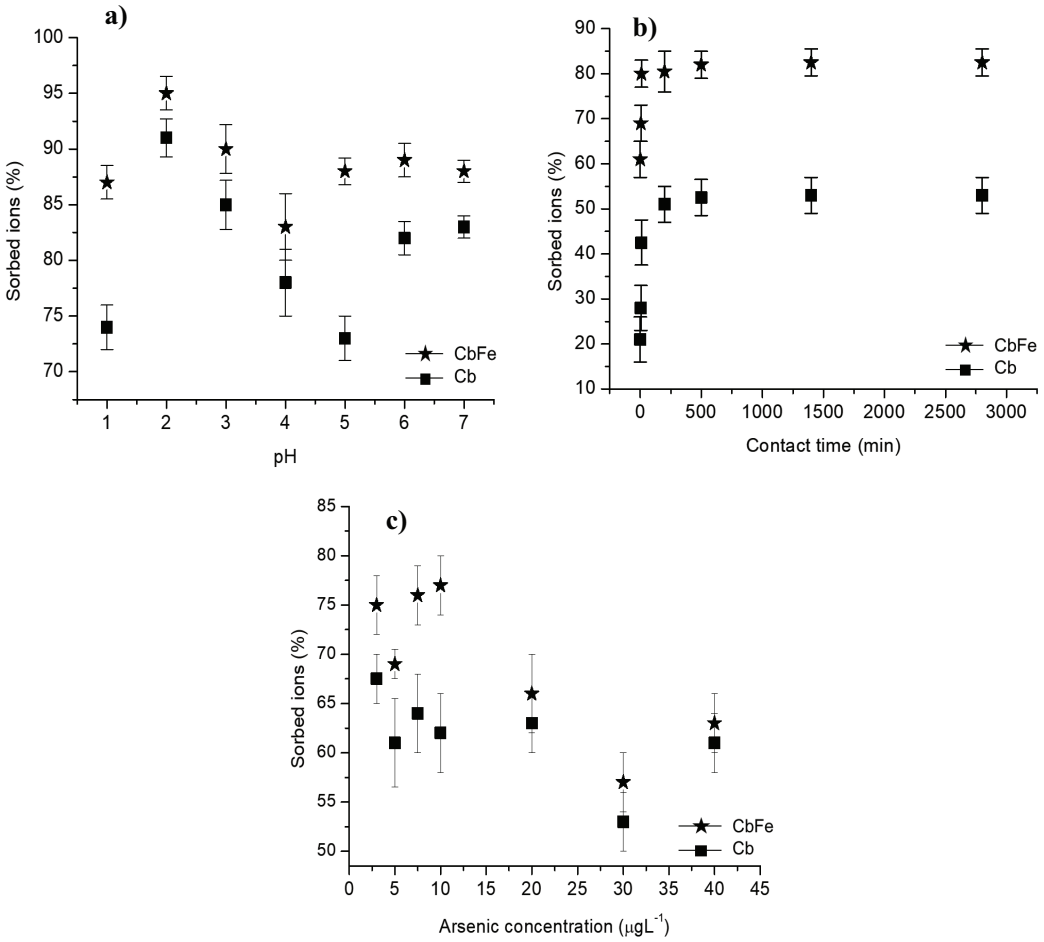

Fig. 4. (a) Effect of pH in the removal of As(V) by Cb and CbFe materials; (b) Percentage of As(V) removed from aqueous solutions by Cb and CbFe in function of time (C_i = 30 mg L^{-1}); (c) Effect of concentration on the removal of As(V) by the Cb and CbFe materials.

Table 2
Fitted kinetic parameters for the removal of As(V) by Cb and CbFe materials

Parameter	Pseudo-first-order		Pseudo-second-order		Diffusion-chemisorption	
	CbFe	Cb	CbFe	Cb	CbFe	Cb
R^2	0.750	0.906	0.999	0.995	0.980	0.980
q_e (mg/g)	0.099	0.075	0.138	0.097	0.159	0.118
k (g/mg min)	9.9959×10^{-4}	5.4451×10^{-4}	0.208	0.098	0.172	0.065

Table 3
Values of Langmuir and Freundlich constants for the As(V) removal

Cb		CbFe	
Freundlich	Langmuir	Freundlich	Langmuir
R^2 = 0.967	R^2= 0.134	R^2 = 0.879	R^2 = 0.593
K_f = 2.126	$1/Q_mK$ = 0.548	K_f = 4.332	$1/Q_mK$ = 0.302
$1/n$ = 0.884	$1/Q_m$ = 0.005	$1/n$ = 0.718	$1/Q_m$ = 0.011

represents a great advantage to remove arsenic in an aqueous phase. Also due to its sorption properties, it represents a great advantage to remove arsenic in an aqueous phase.

4. Adsorption mechanism

After the arsenic contact, an analysis by FTIR was performed (Fig. 2(i)), and the difference between intensity of some bands were observed with respect to Fig. 2(h): 2,362–2,334 cm^{-1}; 1,055 cm^{-1} and 670 cm^{-1} as well as shifting of Fe–O suggesting that these groups are involved in the process of arsenic remotion [48]. According to the results obtained, the process of removal of As(V) can be explained by two ways: chemisorptions on the active site of surface and ion-exchange of surface cations, such as Na^{2+} and Ca^{2+}. The sorption mechanism of As(V) was carried out by Na^{+} and Ca^{+} with As(V), which was confirmed from the SEM-EDX studies (Table 5) [49].

Table 4
Maximum adsorption capacities of various adsorbents for As(V) removal

Adsorbents	Adsorption capacity (mg g^{-1})	Reference
Aluminium-manganese copper ferrite polymer	0.053	[50]
Biochar-supported zerovalent iron	124.50	[51]
Zerovalent iron impregnated chitosan-carboxymethyl β-cyclodextrin	13.51	[52]
Iron oxide on activated carbon	27.78	[53]
Iron-PVA	87.18	[54]
Iron clinoptilolite-rich zeolitic tuff	230	[55]
This work	138.5	–

Table 5
EDX analysis of CFe and CFe-As

Element	CFe %w	CFe-As %w
C	75.92	76.31
O	16.03	18.62
Na	1.60	0.18
Mg	0.23	
Si	1.04	1.06
Al	0.20	0.05
Ca	1.44	0.64
P	0.56	0.52
S	0.54	0.55
K	0.43	
Fe	2.01	2.07

5. Conclusion

In this research, a novel carbonaceous material with iron nanoparticles coming from the pineapple peel (*Ananas comosus* (L.) Merr.) was obtained. SEM results show the presence of three different structures: spheres, filaments and iron nanoparticles distributed on the carbon surface with an average diameter of 38.81 nm. The carbonaceous material with iron nanoparticles (CbFe) and the carbon material (Cb) presented a specific area of 167.00 and 98.80 m^2/g, density sites 7.12 ± 1 sites/nm^2 and 5 ± 1 sites/nm^2 and isoelectric point at pH = 11 and pH = 10.6, respectively. Major differences by means of FTIR analysis between CP, Cb and CbFe were found due mainly to the loss of phenolic compounds during the pineapple peel conditioning and the formation of carboxymethyl–iron complex. In the CbFe material, isonitrile and isocyanate groups were identified as the common functional carbon groups. The capacity of the carbon (Cb) and carbonaceous with iron nanoparticle (CbFe) materials for the As(V) removal were evaluated. Both materials reached the kinetic equilibrium in the first 8 h of contact time, removing 138.5 mg/g of As by the CbFe material and 96.95 mg of As by the Cb material. Kinetic data were properly adjusted to the pseudo-second-order model, indicating that the As(V) removal is due to a chemisorption process, however, this behaviour may be affected by change in pH. Adsorption isotherms for CbFe and Cb materials were adjusted to the Freundlich model resulting in a correlation coefficient R^2 = 0.8797 and R^2 = 0.9671, respectively, which indicates multi-layer chemisorptions of As(V) in a heterogeneous medium. The FTIR characterization of the solid material after the adsorption process indicates that isonitrile groups C–O and C–H are involved in the adsorption process. The carbonaceous material conditioned with iron nanoparticles is a viable option for the As(V) adsorption in an aqueous phase.

Acknowledgements

The authors would like to acknowledge Jorge Pérez for their technical assistance. D.O. Flores-Cruz acknowledges CONACYT for the M.S. fellowship received in support of this work.

Conflict of interest

The authors declared no conflict of interest.

References

[1] S. Chena, D. Wu, Adapting ecological risk valuation for natural resource damage assessment in water pollution, Environ. Res., 164 (2018) 85–92.
[2] M.I. Litter, M. Morgada, J. Bundschuh, Possible treatments for arsenic removal in Latin America waters for human consumption, Environ. Pollut., 158 (2010) 1105–1118.
[3] J.C. Ng, J. Wang, A. Shraim, A global health problem caused by arsenic from natural sources, Chemosphere, 352 (2000) 1353–1359.
[4] Secretaría de Salud, Modificación a la Norma Oficial Mexicana NOM-127-SSA1-1994, Salud ambiental, Agua para uso y consumo humano. Límites permisibles de calidad y tratamientos a que debe someterse el agua para su potabilización, Diario Oficial de la Federación, Miércoles 22 de noviembre de 2000.
[5] M. Bilici-Baskan, A. Pala, A statistical experiment design approach for arsenic removal by coagulation process using aluminum sulfate, Desalination, 254 (2010) 42–48.
[6] H. Strathman, Electrodialysis, a mature technology with a multitude of new applications, Desalination, 264 (2010) 268–288.
[7] J.F. Martínez-Villafañe, C. Montero-Ocampo, A.M. García-Lara, Energy and electrode consumption analysis of electrocoagulation for the removal of arsenic from groundwater, J. Hazard. Mater., 172 (2009) 1617–1622.
[8] M. Sen, A. Manna, P. Pal, Removal of arsenic from contaminated groundwater by membrane-integrated hybrid treatment system, J. Membr. Sci., 354 (2010) 108–113.
[9] S. Alvarado, M. Guédez, M.P. Lué-Merú, G. Nelson, A. Alvaro, A.C. Jesús, Z. Gyula, Arsenic removal from waters by bioremediation with the aquatic plant Water Hyacinth (*Eichhornia crassipes*) and Lesser Duckweed (*Lemna minor*), Bioresour. Technol., 99 (2008) 8436–8440.
[10] D. Mohan, Jr., C.U. Pittman, Arsenic removal from water/wastewater using adsorbents - a critical review, J. Hazard. Mater., 142 (2007) 1–53.

[11] Z.O. Kocabas, Y. Yürüm, Kinetic modeling of arsenic removal from water by ferric ion loaded red mud, Sep. Sci. Technol., 46 (2011) 2380–2390.
[12] Y. Kim, C. Kim, I. Choi, S. Rengaraj, J. Yi, Arsenic removal using mesoporous alumina prepared via a templating method, Environ. Sci. Technol., 38 (2004) 924–931.
[13] K. Upendra, Agricultural products and by-products as a low cost adsorbent for heavy metal removal from water and wastewater, a review, Sci. Res. Essay, 1 (2006) 33–37.
[14] H. Dong, X. Guan, I.M.C. Lo, Fate of As (V)-treated nano zero-valent iron: determination of arsenic desorption potential under varying environmental conditions by phosphate extraction, Water Res., 468 (2012) 4071–4080.
[15] V. Zaspalis, A. Pagana, S. Sklari, Arsenic removal from contaminated water by iron oxide sorbents and porous ceramic membranes, Desalination, 217 (2007) 167–180.
[16] A. Saritha, B. Raju, D. Narayana Rao, A. Roychowdhury, D. Das, K.A. Hussain, Facile green synthesis of iron oxide nanoparticles via solid-state thermolysis of a chiral, 3D anhydrous potassium tris(oxalato) ferrate(III) precursor, Adv. Powder Technol., 26 (2015) 349–354.
[17] T. Wang, J. Lin, Z. Chen, M.R. Megharaj Naidu, Green synthesized iron nanoparticles by green tea and eucalyptus leaves extracts used for removal of nitrate in aqueous solution, J. Clean. Prod., 83 (2014) 413–419.
[18] X.Q. Li, D.W. Elliott, W.X. Zhang, Zero-valent iron nanoparticles for abatement of environmental pollutants, materials and engineering aspects, Crit. Rev. Solid State Mater. Sci., 31 (2006) 111–122.
[19] G.E. Hoag, J.B. Collins, J.L. Holcomb, J.R. Hoag, M.N. Nadagouda, R.S. Varma, Degradation of bromothymol blue by 'greener' nano-scale zero-valent iron synthesized using tea polyphenols, J. Mater. Chem., 19 (2009) 8671–8677.
[20] V. Madhavi, T.N.V.K.V. Prasad, A.V.B. Reddy, B.R. Reddy, G. Madhavi, Application of phytogenic zerovalent iron nanoparticles in the adsorption of hexavalent chromium, Spectrochim. Acta, 116 (2013) 17–25.
[21] V. Smuleac, R. Varma, S. Sikdar, D. Bhattacharya: green synthesis of Fe and Fe/Pd bimetallic nanoparticles in membranes for reductive degradation of chlorinated organics, J. Membr. Sci., 379 (2011) 131–137.
[22] Z. Es'haghi, F. Vafaeinezhad, S. Hooshmand, Green synthesis of magnetic iron nanoparticles coated by olive oil and verifying its efficiency in extraction of nickel from environmental samples via UVVis spectrophotometry, Process Safety Environ. Protect., 102 (2016) 403–409.
[23] T.M.S. Attia, X.L. Hu, D.Q. Yin, Synthesised magnetic nanoparticles coated zeolite (MNCZ) for the removal of arsenic (As) from aqueous solution, J Exp. Nanosci., 9 (2014) 2075–2085.
[24] P.V.R.K. Praveen Kumar, G.K.P. Ramacharyulu, B. Singh, Montmorillonites supported with metal oxide nanoparticles for decontamination of sulfur mustard, Appl. Clay Sci., 116–117 (2015) 263–272.
[25] J. Reddy Koduru, Y.Y. Chang, J.K. Yang, I.S. Kim, Iron oxide impregnated *Morus alba* L. fruit peel for biosorption of Co(II): biosorption properties and mechanism, Sci. World J., 2013 (2013) 1–14.
[26] M. Nairat, T. Shahwan, A.E. Erog˘lu, H. Fuchs, Incorporation of iron nanoparticles into clinoptilolite and its application for the removal of cationic and anionic dyes, J. Ind. Eng. Chem., 21 (2015) 1143–1151.
[27] H.S. Park, J.R. Koduru, K.H. Choo, B. Lee, Activated carbons impregnated with iron oxide nanoparticles for enhanced removal of bisphenol A and natural organic matter, J. Hazard. Mater., 286 (2016) 315–324.
[28] F. Yu, J. Ma, J. Wang, M. Zhang, J. Zheng, Magnetic iron oxide nanoparticles functionalized multi-walled carbon nanotubes for toluene, ethylbenzene and xylene removal from aqueous solution, Chemosphere, 146 (2016) 162–172.
[29] A. Yadav, A.K. Teja, N. Verma, Removal of phenol from water by catalytic wet air oxidation using carbon bead supported iron nanoparticle containing carbon nanofibers in an especially configured reactor, J. Environ. Chem. Eng., 4 (2016) 1504–1513.
[30] W. Wang, Y. Cheng, T. Kong, G. Cheng, Iron nanoparticles decoration onto three-dimensional graphene for rapid and efficient degradation of azo dye, J. Hazard. Mater., 299 (2015) 50–58.
[31] H. Jabeen, V. Chandra, S. Jung, J.W. Lee, K.S.B. Kim, Enhanced Cr(VI) removal using iron nanoparticle decorated graphene, Nanoscale, 3 (2011) 3583–3585.
[32] J. Guo, R. Wang, W.W. Tjiu, J. Pan, T. Liu, Synthesis of Fe nanoparticles@graphene composites for environmental applications, J. Hazard. Mater., 225–226 (2012) 63–73.
[33] G.C. D'Eeckenbrugge, F. Leal, R.E. Paull, K.G. Rohrbach, Chapter 2 Morphology, Anatomy and Taxonomy, in D.P. Bartholomew, Ed., The Pineapple, Botany, Production and Uses, CABI Publishing, 2003, pp. 13–32.
[34] K.S.W. Sing, D.H. Everett, R.A.W. Haul, L. Moscou, R.A. Pierotti, J. Rouquerol, T. Siemieniewska, Reporting physisorption data for gas/solid systems with special reference to the determination of surface area and porosity, Pure Appl. Chem., 57 (1985) 603–619.
[35] M.S. De Celis, J.P. Villaverde, A.L. Cukierman, N.E. Amadeo, Oxidative dehydrogenation of ethylbenzene to styrene on activated carbons derived from a native wood as catalyst, Lat. Am. Appl. Res., 39 (2009) 165–171.
[36] J.C.P. Vaghetti, E.C. Lima, B. Royer, B.M. Cunha, N.F. Cardoso, J.L. Brasil, S.L.P. Dias, Pecan nutshell as biosorbent to remove Cu(II) and Pb(II) from aqueous solutions, J. Hazard. Mater., 162 (2009) 270–280.
[37] K. Ishimaru, T. Hata, P. Bronsveld, D. Meier, Y. Imamura, Spectroscopic analysis of carbonization behavior of wood, cellulose and lignin, J. Mater. Sci., 42 (2007) 122–129.
[38] A. Atrens, A.S. Lim, ESCA studies of nitrogen-containing stainless steels, J. Appl. Phys. A, 51 (1990) 411–418.
[39] Y.H. Lin, H.H. Tseng, M.Y. Wey, M.D. Lin, Characteristics of two types of stabilized nano zero-valent iron and transport in porous media, Sci. Total Environ., 408 (2010) 2260–2267.
[40] P.L. Smedley, D.G. Kinniburgh, A review of the source, behaviour and distribution of arsenic in natural waters, Appl. Geochem., 17 (2002) 517–568.
[41] H. Zhu, Y. Jia, X. Wu, H. Wang, Removal of arsenic from water by supported nano zero-valent iron on activated carbon, J. Hazard. Mater., 172 (2009) 1591–1596.
[42] S.R. Chowdhury, A.R. Pratt, E.K. Yanful, Arsenic removal from aqueous solutions by mixed magnetite-maghemite nanoparticles, Environ. Earth Sci., 64 (2011) 411–423.
[43] Z. Liu, F.S. Zhang, R. Sasai, Arsenate removal from water using Fe_3O_4-loaded activated carbon prepared from waste biomass, Chem. Eng. J., 160 (2010) 57–62.
[44] M.G. Mostafa, Y.H. Chen, J.S. Jean, C.C. Liu, Y.C. Lee, Kinetics and mechanism of arsenate removal by nanosized iron oxide-coated perlite, J. Hazard. Mater., 187 (2001) 89–95.
[45] C. Sutherland, C. Venkobachar, A diffusion-chemisorption kinetic model for simulating biosorption using forest macro fungus *Fomes fasciatus*, Int. Res. J. Plant Sci., 1 (2010) 107–117.
[46] S. Bang, G.P. Korfiatis, X. Meng, Removal of arsenic from water by zero-valent iron, J. Hazard. Mater., 121 (2005) 61–67.
[47] D.G.J. Mann, N. Labbé, R.W. Sykes, K. Gracom, L. Kline, I.M. Swamidoss, J.N. Burris, M. Davis, C.N. Jr Stewart, Rapid assessment of lignin content and structure in switchgrass (*Panicum virgatum*) grown under different environmental conditions, Bioenergy Res., 2 (2009) 246–256.
[48] L. Prasanna Lingamdinne, J. Reddy Koduru, Y.-L., Y.Y. Chang, J.K. Yang, Studies on removal of Pb(II) and Cr(III) using graphene oxide based inverse spinel nickel ferrite nano-composite as sorbent, Hydrometallurgy, 165 (2016) 64-72.
[49] H. Roh, M.R. Yu, K. Yakkala, J. Reddy Koduru, J.K. Yang, Y.Y. Chang, Removal studies of Cd(II) and explosive compounds using buffalo weed biochar-alginate beads, J. Ind. Eng. Chem., 26 (2015) 226–233.
[50] M. Aslam Malana, R. Beenish Qureshi, M. Naeem Ashiq, Adsorption studies on nano aluminium doped manganese copper ferrite polymer (MA, VA, AA) composite: kinetic and mechanism, Chem. Eng. J., 172 (2001) 721–727.

[51] S. Wang, B. Gao, Y. Li, A.E. Creamer, F. He, Adsorptive removal of arsenate from aqueous solutions by biocharsupported zero-valent iron nanocomposite: batch and continuous flow tests, J. Hazard. Mater., 322 (2017) 172–181.
[52] M.T. Sikder, S. Tanaka, T. Saito, M. Kurasaki, Application of zerovalent iron impregnated chitosan-carboxymethyl-β-cyclodextrin composite beads as arsenic sorbent, J. Environ. Chem. Eng., 2 (2014) 370–376.
[53] A. Yürüm, Z.Ö. Kocabas-Atakl, M. Sezen, R. Semiat, Y. Yurum, Fast deposition of porous iron oxide on activated carbon by microwave heating and arsenic (V) removal from water, Chem Eng J 242 (2014) 321-332.
[54] A. Santos, F.W. Ferreira de Oliveira, F.H. Araujo Silva, D.A. Maria, AJ Domingos, W.A. De Almeida Macêdo, H.E. Leonhardt Palmieri, Batista M. Franco, Synthesis and characterization of iron-PVA hydrogel microspheres and their use in the arsenic (V) removal from aqueous solution, Chem. Eng. J., 210 (2012) 432–443.
[55] M.M. Dávila-Jiménez, M.P. Elizalde-González, J. Mattusch, P. Morgenstern, M.A. Pérez-Cruz, Y. Reyes-Ortega, R. Wennrich, H. Yee-Madeira, In situ and ex situ study of the enhanced modification with iron of clinoptilolite-rich zeolitic tuff for arsenic sorption from aqueous solutions, J. Colloid Interface Sci., 322 (2008) 527–536.